MIMO Radar Detection of Targets in Compound-Gaussian Clutter

Murat Akcakaya, Martin Hurtado, and Arye Nehorai

Electrical and Systems Engineering Department.
Washington University in St.louis
St.louis, Missouri 63130
Emails: makcak2, mhurta3, nehorai@ese.wustl.edu

***Abstract*—Multiple-input multiple-output (MIMO) radars with widely-separated transmitters and receivers are useful to discriminate a target from clutter using the spatial diversity of the scatterers in the illuminated scene. We consider the detection of targets in compound-Gaussian clutter fitting for example scatterers with heavy-tailed distributions for high-resolution and/or low-grazing-angle radars in the presence of sea or foliage clutter. First, we introduce a data model using the inverse gamma distribution to represent the clutter texture. Then, we apply the parameter-expanded expectation-maximization (PX-EM) algorithm to estimate the clutter texture and speckle, as well as the target parameters. We develop a generalized likelihood ratio (GLR) test target detector using the estimates and show the advantages of MIMO using Monte Carlo simulations.**

I. Introduction

Multiple-input multiple-output (MIMO) radar refers to a system using spatially distributed transmitters and jointly processing the received signals at multiple receivers. MIMO radar has been investigated under two possible configurations: (i) colocated [1] and (ii) widely-separated antennas [2]. With colocated antennas, the radar system is shown to have improved detection performance and higher resolution [3], higher sensitivity for detecting moving targets [4], radiation pattern with lower side lobes and better suppression [5].

MIMO radars with widely-separated antennas, exploit the spatial diversity and take the advantage of the spatial properties of targets' radar cross section (RCS). The RCS of the complex radar targets are quickly changing functions of the angle aspect. These target scintillations cause signal fading and deteriorates the radar performance. When the transmitters are sufficiently separated, the multiple signals illuminate the target from de-correlated angles, and hence each signal carries independent information. This spatial diversity improves the radar performance by mitigating these scintillations. These systems have the ability to: support high resolution target localization [6]; improve the target parameter estimation [7], and detection performance [8]; handle slow moving targets by exploiting Doppler estimates from multiple directions [9], [10]. Here we focus on MIMO radar with widely distributed antennas for target detection. Therefore, for simplicity, in the rest of the paper by MIMO we refer to a system with widely separated antennas.

MIMO radar systems can be further categorized into two processing modes (coherent and non-coherent) depending on the need for phase synchronization [11]. In this paper we consider the case of coherent processing by assuming that the phase difference between each transmitter and receiver pair is available. The non-coherent case is left for subsequent work.

Target detection for MIMO systems has been addressed with white and colored Gaussian noise in [8] and [12], respectively. However, real clutter often deviates from complex Gaussian model. Then, this conventional model cannot represent the heavy-tailed clutter statistics which are distinctive of several scenarios, e.g., high-resolution and/or low-grazing-angle radars in the presence of sea or foliage clutter [13], [14]. Therefore, in this work, we assume that the clutter reflections at the receiver follow compound-Gaussian model $\boldsymbol{e} = \sqrt{u}\mathcal{X}$, where u and $\mathcal{X}$ are the texture and speckle components of the compound model, respectively. The fast-changing $\mathcal{X}$ is a realization of a stationary zero mean complex Gaussian process; and the slow-changing u is modeled as a nonnegative real random process [15].

Clutter modeling with compound-Gaussian distribution requires the selection of the texture characteristics. Gamma distribution for the texture is investigated in [16] for MIMO radar systems leading to the well-known K clutter model. In this work, we specifically consider the inverse gamma distribution for the texture component u, since it fits well real clutter data [17]. Moreover this choice of distribution results in a closed-form maximum likelihood solution for the joint target and clutter estimation [18].

We also demonstrate the constant-false alarm rate (CFAR) properties of the detection algorithm for the MIMO radar system. In [12] and [16], the detectors support the CFAR property in terms of the clutter covariance using the secondary data obtained from neighboring cells. We do not assume any knowledge about the target and clutter parameters, and without depending on the secondary data we numerically illustrate the CFAR properties of our detector in terms of clutter covariance with our numerical examples.

This work was supported by the ONR Grant N000140810849 and the Department of Defense under the Air Force Office of Scientific Research MURI Grant FA9550-05-1-0443.

The rest of the paper is organized as follows. In Section II, we introduce our parametric measurement model under the generalized multivariate analysis of variance (GMANOVA) framework [19] for the MIMO system. In Section III, we first present a parameter-expanded expectation-maximization (PX-EM) algorithm [20] with the use of the powerful GMANOVA tools to estimate the target and clutter parameters. Then using these estimates we develop a GLR detection test [21]. We analyze the detection performance of this test in Section IV using Monte Carlo simulations.

II. Radar Model

In this section, we develop measurement and statistical models for a coherent MIMO radar system. Our goal is to present an algorithm, under GMANOVA framework, for detection of a target in the range cell of interest (COI), when the signal and noise parameters are unknown.

A. Measurement Model

We consider an antenna system with M transmitters and N receivers, assuming narrow-band signals. We define $(x_{\mathrm{T}_m}, y_{\mathrm{T}_m})$, $m = 1, ..., M$ and $(x_{\mathrm{R}_n}, y_{\mathrm{R}_n})$, $n = 1, ..., N$ as the locations of the transmitters and receivers, respectively. Moreover, we assume that the target in the COI is composed of multiple scatterers as in [8]. However, since the transmitted waveforms cannot resolve the individual scatterers due to bandwidth assumptions, the reflections from the target can be assumed to come from a single scatterer located at (x_0, y_0) (point target), which is the RCS center of gravity of these multiple scatterers. Then, we write the vector of baseband received signals following [2] and [8]:

$$\boldsymbol{r}(t) = \mathrm{diag}(\boldsymbol{a}(x_0, y_0))H\mathrm{diag}(\boldsymbol{b}(x_0, y_0))\boldsymbol{s}(t - \tau_0) + \boldsymbol{\epsilon}(t), \quad (1)$$

where

- $\boldsymbol{r}(t) = [r_1(t), ..., r_{_N}(t)]^T$, "$(\cdot)^T$" denotes the transpose,
- H is an $N \times M$ channel matrix such that $[H]_{nm} = h_{nm}$ is the channel coefficient from the m^{th} transmitter to n^{th} receiver corresponding to the target in the COI,
- $\mathrm{diag}(v)$ is a diagonal matrix with v on the diagonal,
- $\boldsymbol{\epsilon}(t)$ is additive clutter noise,
- $\boldsymbol{s}(t - \tau_0) = [s_1(t - \tau_0), ..., s_{_M}(t - \tau_0)]^T$ is the vector of complex envelope of the delayed transmitted signals with $\tau_0 = \tau(x_{\mathrm{T}_1}, y_{\mathrm{T}_1}, x_0, y_0) + \tau(x_{\mathrm{R}_1}, y_{\mathrm{R}_1}, x_0, y_0)$,
- $\boldsymbol{a}(x_0, y_0) = [1, e^{-j\psi_2}, ..., e^{-j\psi_{_N}}]^T$ is the receiver steering vector with $\psi_n = 2\pi f_{\mathrm{c}}[\tau(x_{\mathrm{R_n}}, y_{\mathrm{R_n}}, x_0, y_0) - \tau(x_{\mathrm{R}_1}, y_{\mathrm{R}_1}, x_0, y_0)]$,
- $\boldsymbol{b}(x_0, y_0) = [1, e^{-j\zeta_2}, ..., e^{-j\zeta_{_M}}]^T$ is the transmitter steering vector with $\zeta_m = 2\pi f_{\mathrm{c}}[\tau(x_{\mathrm{T_m}}, y_{\mathrm{T_m}}, x_0, y_0) - \tau(x_{\mathrm{T}_1}, y_{\mathrm{T}_1}, x_0, y_0)]$,
- f_{c} is the carrier frequency of the transmitted signal,
- $\tau(x, y, x', y') = \sqrt{(x - x')^2 + (y - y')^2}/c$, and c is the speed of the signal propagation in the medium.

The measurements in (1) are the superposition of the scaled and delayed versions of the M different transmitted signals. Therefore, in order to discriminate the measurements at the receiver corresponding to different transmitted signals, we consider orthogonality among the transmitted waveforms. Moreover, we assume that this orthogonality is maintained for different mutual delays [2]: $\int_{T_{\mathrm{s}}} s_m(t)s^*_{m'}(t - \nu)\mathrm{d}t = 0$ for $m \neq m^{'} = 1, ..., M$, where T_{s} is the pulse length. Under these assumptions, we apply matched-filtering corresponding to the signal $s_m(t)$ and obtain the $N \times 1$ measurement vector for a single pulse as

$$\begin{aligned} \tilde{\boldsymbol{r}}_m &= \int_{T_{\mathrm{s}}} \boldsymbol{r}(t)s^*_m(t - \tau_0)\mathrm{d}t \\ &= \mathrm{diag}(\boldsymbol{a}(x_0, y_0))\boldsymbol{h}_m e^{-j\zeta_m} + \tilde{\boldsymbol{\epsilon}}_m, \end{aligned} \quad (2)$$

where $\boldsymbol{h}_m$ is the m^{th} column of the channel matrix H, and $\tilde{\boldsymbol{\epsilon}}_m$ is the clutter output. We stack the matched-filter outputs $\tilde{\boldsymbol{r}}_m$, $m = 1, ..., M$ into an $NM \times 1$ vector

$$\begin{aligned} \boldsymbol{y} &= [\tilde{\boldsymbol{r}}_1^T,\ \tilde{\boldsymbol{r}}_2^T,\ \ldots,\ \tilde{\boldsymbol{r}}_M^T]^T + \boldsymbol{e} \\ &= A\boldsymbol{x}\phi + \boldsymbol{e}, \end{aligned} \quad (3)$$

where

- $A = \mathrm{diag}(\boldsymbol{b}(x_0, y_0)) \otimes \mathrm{diag}(\boldsymbol{a}(x_0, y_0))$,
- $\boldsymbol{x} = [\boldsymbol{h}_1^T,\ \boldsymbol{h}_2^T,\ \ldots,\ \boldsymbol{h}_M^T]^T$,
- $\phi = 1$,
- and $\boldsymbol{e} = [\tilde{\boldsymbol{\epsilon}}_1^T,\ \tilde{\boldsymbol{\epsilon}}_2^T,\ \ldots,\ \tilde{\boldsymbol{\epsilon}}_M^T]^T$.

We transmit K pulses and assume that the target is stationary during this observation time, then

$$Y = [\boldsymbol{y}(1)\ \boldsymbol{y}(2)\ \ldots\ \boldsymbol{y}(K)]_{_{NM\times K}} = A\boldsymbol{x}\boldsymbol{\phi} + E, \quad (4)$$

where

- $\boldsymbol{\phi} = [\phi(1),\ \ldots,\ \phi(K)] = [1,\ \ldots,\ 1]_{1\times K}$,
- $E = [\boldsymbol{e}(1)\ \boldsymbol{e}(2)\ \ldots\ \boldsymbol{e}(K)]_{_{NM\times K}}$ is the additive noise.

B. Statistical Model

We assume that the vector $\boldsymbol{x}$ in (4), composed of the channel coefficients h_{nm}, is unknown deterministic; this is different than the stochastic approach taken by the authors of [8], meaning that we do not make any assumptions on channel coefficients. The matrix A in (4) is known due to the coherent processing assumption. Moreover, we consider the compound-Gaussian distribution $\boldsymbol{e}(k)$=$\sqrt{u(k)}\mathcal{X}(k)$, $k = 1, ..., K$ to model the clutter with $u(k)$ and $\mathcal{X}(k)$ as the texture and speckle components, respectively see [18] and references therein. Recall that the realizations of the fast-changing component, $\mathcal{X}(k)$, $k = 1, ..., K$ are independent and identically distributed (i.i.d.) and follow Gaussian distribution with zero mean and covariance Σ. The texture is the slow-changing component [15], and thus we consider it to be constant during the pulse duration T_{s}. However, we also assume the texture to be independent realizations of the same random process from pulse to pulse, *i.e.,* $\mathrm{Cov}(u(k), u(k^{'})) = 0$ for $k \neq k^{'}$ [22]. Therefore, $\boldsymbol{e}(k)$ $k = 1, ..., K$ are i.i.d., and we can write the conditional distribution for the observation Y in (4) as

$$\begin{aligned} \prod_{k=1}^{K} p_{\boldsymbol{y}|u}(\boldsymbol{y}(k)|u(k)) &= \prod_{k=1}^{K} \frac{1}{|\pi u(k)\Sigma|} \exp\Big\{ - [\boldsymbol{y}(k) - A\boldsymbol{x}\phi(k)]^H \\ &\quad \cdot [u(k)\Sigma]^{-1} [\boldsymbol{y}(k) - A\boldsymbol{x}\phi(k)] \Big\}, \end{aligned} \quad (5)$$

where"$(\cdot)^H$" denotes the Hermitian transpose.

Observe that with known A and $\boldsymbol{\phi}$, and unknown $\boldsymbol{x}$ and Σ, (4) is a GMANOVA model. We assume that $w(k) = 1/u(k)$ follows the gamma distribution (consequently $u(k)$ follows inverse gamma distribution) with unit mean and unknown shape parameter $v > 0$ as in [18], *i.e.,*

$$p_w(w(k); v) = \frac{1}{\Gamma(v)} v^v w(k)^{v-1} \exp\left[-vw(k)\right], \qquad (6)$$

where $\Gamma(\cdot)$ is the gamma function. Therefore, we consider $\boldsymbol{x}$, Σ and v as the unknown parameters.

III. Detection and Estimation Algorithms

We present, in this section, maximum likelihood estimation (MLE) of the unknown parameters and target detection test. We derive a GLR test using the complete data likelihood function, with Y as observed and $u(k)$, $k = 1, \ldots, K$ as unobserved data to decide about the presence of a target in the COI. Namely, we choose between two hypotheses in the following parametric test

$$\begin{cases} \mathcal{H}_0 : & \boldsymbol{x} = \mathbf{0}, \Sigma, v \\ \mathcal{H}_1 : & \boldsymbol{x} \neq \mathbf{0}, \Sigma, v \end{cases}, \qquad (7)$$

with the speckle covariance Σ and the inverse texture shape parameter v as the nuisance parameters. We compute the GLR test by replacing the unknown parameters with their MLEs in the likelihood ratio test. Then, we reject $\mathcal{H}_0$ (target-free case) in favor of $\mathcal{H}_1$ (target-present case) when

$$\mathrm{GLR} = \frac{p_1(Y, u(1), \ldots, u(K); \hat{\boldsymbol{x}}_1, \hat{\Sigma}_1, \hat{v}_1)}{p_0(Y, u(1), \ldots, u(K); \hat{\Sigma}_0, \hat{v}_0)} > \eta, \qquad (8)$$

where $p_0(\cdot)$ and $p_1(\cdot)$ are the complete data likelihood functions under $\mathcal{H}_0$ and $\mathcal{H}_1$. Moreover, $\hat{\Sigma}_0$ and $\hat{\Sigma}_1$, are the MLEs of Σ, and $\hat{v}_0$ and $\hat{v}_1$ are the MLEs of the shape parameter v under $\mathcal{H}_0$ and $\mathcal{H}_1$; $\hat{\boldsymbol{x}}_1$ is the MLE of $\boldsymbol{x}$ under $\mathcal{H}_1$; η is the detection threshold.

We compute the MLEs of the vector $\boldsymbol{x}$, speckle covariance matrix Σ and texture distribution shape parameter v using the hierarchical data model presented in (5) and (6). We consider two iterative loops for the MLE computations: (i) inner loop and (ii) outer loop. In the inner loop, first we introduce the PX-EM algorithm to obtain the MLE estimates $\hat{\boldsymbol{x}}$ and $\hat{\Sigma}$ for a fixed v. The PX-EM algorithm has the same convergence properties as the classical EM algorithm, but it outperforms the EM algorithm in terms of global rate of convergence [20]. In the outer loop, we estimate v using the MLEs from the inner loop [18].

A. Inner Loop

PX-EM Algorithm for Inverse Gamma Texture

Recall that $\boldsymbol{x}$, Σ and v are the unknown parameters. We first estimate $\boldsymbol{\theta} = \{\boldsymbol{x}, \Sigma\}$ assuming that v is known. We implement the PX-EM algorithm by adding a new unknown parameter μ_w, the mean of $w(k)$, to this set, *i.e.*, $\boldsymbol{\theta}_* = \{\boldsymbol{x}, \Sigma_*, \mu_w\}$. In this model, since the maximization step performs a more efficient analysis by fitting the expanded parameter set, PX-EM algorithm has a rate of convergence at least as fast as EM algorithm [20]. Under this expanded model the pdf of $w(k)$ is

$$p_w(w(k); v_*, \mu_w) = \frac{1}{\Gamma(v)} \left(\frac{v}{\mu_w}\right)^v w(k)^{v-1} \exp\left[-vw(k)/\mu_w\right]. \qquad (9)$$

Consider $\boldsymbol{\theta} = R(\boldsymbol{\theta}_*) = \{\boldsymbol{x}, \Sigma_*/\mu_w\}$, where $R(\cdot)$ is the reduction function (many-to-one) from the expanded to the original space. Moreover, $\mu_w^0 = 1$ is the null value such that the complete-data model is preserved.

Since the complete-data likelihood function belongs to an exponential family, we simplify the PX-EM algorithm following [23]. Thus the PX-E step reduces to calculating the conditional expectation of the natural complete-data sufficient statistics given the observed data and expanded unknown parameters with $\mu_w = \mu_w^0$. Then, the PX-M is simply replacing the natural complete-data sufficient statistics in the MLE expressions of $\boldsymbol{x}$, Σ_* and μ_w with their conditional expectations obtained in the PX-E step.

We find the expressions for the MLEs of $\boldsymbol{x}$, Σ_* and μ_w using the complete data log-likelihood function. These MLEs can be shown to be functions of the natural complete-data sufficient statistics. Since (4) is a GMANOVA model, we use the results of [19] for the MLEs of $\boldsymbol{x}$ and Σ_*. We skip the detailed derivation in this paper due to space limitations, for further explanation see [18, Appendix A].

We define i and j as the inner and outer loop iteration indexes, respectively. We summarize the algorithm:

PX-E Step: Calculate the conditional expectation of the sufficient statistics under $\mathcal{H}_1$, concentrated at $\hat{v}^{(j)}$, the j^{th} iteration step estimate of v

$$T_1^{(i)} = \frac{1}{K}\sum_{k=1}^{K} \boldsymbol{y}(k)\phi(k)^H \cdot \mathrm{E}_{w|y}[w(k)|\boldsymbol{y}(k); \hat{\boldsymbol{\theta}}_*^{(i)}, \hat{v}^{(j)}], \qquad (10a)$$

$$T_2^{(i)} = \frac{1}{K}\sum_{k=1}^{K} \boldsymbol{y}(k)\boldsymbol{y}(k)^H \cdot \mathrm{E}_{w|y}[w(k)|\boldsymbol{y}(k); \hat{\boldsymbol{\theta}}_*^{(i)}, \hat{v}^{(j)}], \qquad (10b)$$

$$T_3^{(i)} = \frac{1}{K}\sum_{k=1}^{K} \phi(k)\phi(k)^H \cdot \mathrm{E}_{w|y}[w(k)|\boldsymbol{y}(k); \hat{\boldsymbol{\theta}}_*^{(i)}, \hat{v}^{(j)}], \qquad (10c)$$

$$T_4^{(i)} = \frac{1}{K}\sum_{k=1}^{K} \mathrm{E}_{w|y}[w(k)|\boldsymbol{y}(k); \hat{\boldsymbol{\theta}}_*^{(i)}, \hat{v}^{(j)}], \qquad (10d)$$

where $\hat{\boldsymbol{\theta}}_*^{(i)} = \{\hat{\boldsymbol{x}}^{(i)}, \hat{\Sigma}_*^{(i)}, \hat{\mu}_w^{(i)} = \hat{\mu}_w^0 = 1\}$ is the estimate of $\boldsymbol{\theta}_*$ at i^{th} iteration. Using the properties of compound-Gaussian model with inverse gamma distributed texture, we observe that $w(k)|y(k)$ follows gamma distribution, then

$$\mathrm{E}_{w|y}[w(k)|\boldsymbol{y}(k); \hat{\boldsymbol{\theta}}_*^{(i)}] = (\hat{v}^{(j)} + MN) + \left\{\hat{v}^{(j)} \cdot d(k, \hat{\boldsymbol{\theta}}_*^{(i)})\right\}^{-1}, \qquad (11)$$

where $d(k,\hat{\boldsymbol{\theta}}_*^{(i)}) = \left[\boldsymbol{y}(k) - A\hat{\boldsymbol{x}}^{(i)}\phi(k)\right]^H \left[\hat{\Sigma}^{(i)}\right]^{-1} \left[\boldsymbol{y}(k) - A\hat{\boldsymbol{x}}^{(i)}\phi(k)\right]$.

We define $S^{(i)} = T_2^{(i)} - T_1^{(i)}\left(T_3^{(i)}\right)^{-1}\left(T_1^{(i)}\right)^H$ and $Q^{(i)} = A\left[A^H\left(S^{(i)}\right)^{-1}A\right]^{-1}A^H$, then compute

PX-M Step:

$$\hat{\boldsymbol{x}}_1^{(i+1)} = \left[A^H\left(S^{(i)}\right)^{-1}A\right]^{-1}A^H \cdot\left(S^{(i)}\right)^{-1}T_1^{(i)}\left(T_3^{(i)}\right)^{-1}, \tag{12a}$$

$$\hat{\Sigma}_*^{(i+1)} = \left(S^{(i)}\right)^{-1} + \left[I_{MN} - Q^{(i)}\left(S^{(i)}\right)^{-1}\right]T_1^{(i)} \cdot\left(T_3^{(i)}\right)^{-1}\left(T_1^{(i)}\right)^H \cdot\left[I_{MN} - Q^{(i)}\left(S^{(i)}\right)^{-1}\right]^H, \tag{12b}$$

$$\hat{\mu}_w^{(i+1)} = T_4^{(i)}, \tag{12c}$$

$$\hat{\Sigma}_1^{(i+1)} = \hat{\Sigma}_*^{(i+1)}/\hat{\mu}_w^{(i+1)}, \tag{12d}$$

Under $\mathcal{H}_0$, we calculate $\hat{\Sigma}_0$, with $\boldsymbol{x} = \mathbf{0}$, and update the sufficient statistics accordingly.

B. Outer Loop

We compute $\hat{v}^{(j+1)}$, by maximizing the concentrated observed data $(\boldsymbol{y}(k), k = 1,\ldots,K)$ log-likelihood function using the estimates from the PX-EM step. We denote $\hat{\boldsymbol{x}}^{(\infty)}$, $\hat{\Sigma}_0^{(\infty)}$ and $\hat{\Sigma}_1^{(\infty)}$ as the estimates of $\boldsymbol{x}$ and Σ obtained upon the convergence of the inner loop and compute

$$\hat{v}_0^{(j+1)} = \arg\max_v \sum_{k=1}^{K} \ln p_{\boldsymbol{y}}\left(\boldsymbol{y}(k), \hat{\Sigma}_0^{(\infty)}, v\right). \tag{13}$$

$$\hat{v}_1^{(j+1)} = \arg\max_v \sum_{k=1}^{K} \ln p_{\boldsymbol{y}}\left(\boldsymbol{y}(k), \hat{\boldsymbol{x}}_1^{(\infty)}, \hat{\Sigma}_1^{(\infty)}, v\right). \tag{14}$$

The computation of $\hat{v}^{(j+1)}$ necessitates a numerical iteration outside the PX-EM algorithm similar to [18]. For this special case of compound-Gaussian model with inverse gamma texture, it is easy to obtain a closed-form expression for the marginal pdf $p_{\boldsymbol{y}}(\cdot)$ of $\boldsymbol{y}(k)$, which is a complex multivariate t distribution [18]. Using this fact, we find that (13) and (14) lead to the same result for v. Therefore, it can easily be shown that the GLR detection test in (8) reduces to

$$\mathrm{GLR} = \frac{|T_1|}{\left|T_2 - Q\left(S\right)^{-1}T_1\left(T_3\right)^{-1}\left(T_1\right)^{-1}\right|} > \eta', \tag{15}$$

where $|\cdot|$ is the determinant operator.

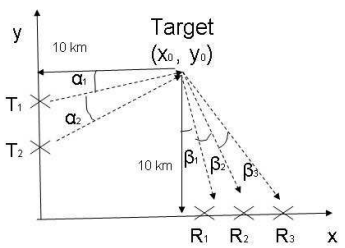

Fig. 1. MIMO antenna system with M transmitters and N receivers.

IV. Numerical Examples

We demonstrate the detection performance of the MIMO radar system with numerical examples using Monte Carlo (MC) simulations. We show the receiver operating characteristics and CFAR properties of the detection algorithm for the MIMO system. The results are obtained from 10^5 MC runs. We follow the scenario shown in Fig. 1. We assume that our system is composed of M transmitters and N receivers, where the antennas are widely separated. The transmitters are located on the y-axis, whereas the receivers are on the x-axis. The target is 10km from each of the axes. The angle between the transmitted signals $\alpha_1 = \alpha_2 = ... = \alpha_M = 10^\circ$ and similarly between the received signals $\beta_1 = ... = \beta_N = 10^\circ$. In this scenario, all the transmitters and receivers see the target from different angles.

We compare the receiver operating characteristics of MIMO radar with conventional phased-array (Conv.) radar in Fig. 2. MIMO MXN and Conv. MXN stand for the MIMO and conventional radar systems, respectively, with M transmitters and N receivers. The model of Conv. radar is obtained from (3) using the fact that all the channel coefficients of the system are the same, since each transmitter and receiver pair sees the target from the same angle. We define the SNR similar to [18]

$$\mathrm{SNR} = \frac{1}{K}\frac{\sum_{k=1}^{K}(A\boldsymbol{x}\phi(k))^H(A\boldsymbol{x}\phi(k))}{\mathrm{E}\{u(k)\}\mathrm{tr}\Sigma}. \tag{16}$$

The channel parameters $\boldsymbol{x}$ and the covariance of the speckle component Σ are chosen randomly for simulation purposes; that is, their entries are assigned as the realizations of zero mean complex Gaussian random variable with unit variance. Later, Σ and $\boldsymbol{x}$ are scaled to meet the desired signal-to-noise ratio (SNR) conditions [22]. The shape parameter is chosen to be $v = 4$. Similar results can be obtained for different v values, but these results are skipped here due to space limitations.

In Fig. 2, we assume $M = 2$ transmitters and $K = 20$ pulses for each transmitted signal. For fairness of comparison, we transmit the same power for all the systems and fix SNR=-15 dB. As expected when the number of the receivers, N, increases, the performances of both MIMO and Conv. radar systems improve. However, MIMO radar always outperforms Conv. radar when both have the same number of receivers. We also show that when $N = 4$ for MIMO radar, the performance of the MIMO system is even better than the Conv. system with $N = 6$ receivers. The observed advantage of MIMO over

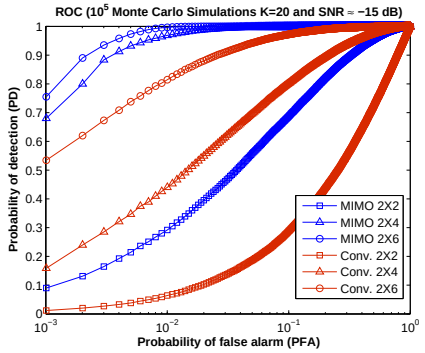

Fig. 2. Receiver operating characteristics of MIMO and conventional phased-array radar (Conv.).

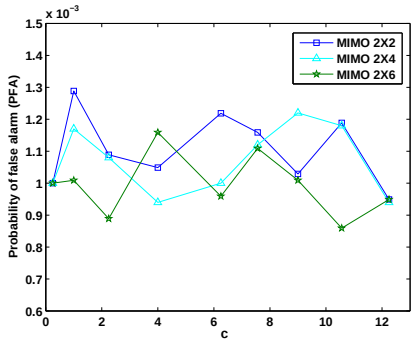

Fig. 3. Probability of false alarm for different covariance values.

Conv. radar stems from the diversity gain obtained by multiple looks at the target with orthogonal signals, that is, MIMO radar systems have the ability to exploit the waveform and spatial diversities, gaining sensitivity about the RCS variations of the target to enhance the system performance.

In Fig. 3, we investigate the CFAR properties of our GLR detector. We set the covariance of the speckle component as $\Sigma^{'} = c\Sigma$. Then, for different values of c, we illustrate the behavior of the probability of false alarm (PFA). We observe that the PFA oscillates around 10^{-3} and there is no significant change in its value; this implies that our detector is CFAR in terms of the covariance of the speckle component.

V. Concluding Remarks

We developed a GLR test target detector for a coherent MIMO radar system in compound-Gaussian clutter with inverse gamma distributed texture when the target and clutter parameters were unknown. First, we introduced a measurement model under the GMANOVA framework, and applied the PX-EM algorithm to estimate the unknown parameters. Using these parameters, we developed the GLR test detector. We demonstrated the performance of our detector using Monte Carlo simulations. We showed the advantage of MIMO over conventional radar for the target detection. Finally, we numerically illustrated that the GLR test detector is CFAR in terms of the speckle covariance. Our future work will concentrate on non-coherent processing of MIMO radar for detection and estimation algorithms.

References

[1] J. Li and P. Stoica, "MIMO radar with colocated antennas," *IEEE Signal Process. Mag.*, vol. 24, pp. 106–114, Sept. 2007.

[2] A. Haimovich, R. Blum, and L. Cimini, "MIMO radar with widely separated antennas," *IEEE Signal Process. Mag.*, vol. 25, pp. 116–129, Jan. 2008.

[3] I. Bekkerman and J. Tabrikian, "Target detection and localization using MIMO radars and sonars," *IEEE Trans. Signal Process.*, vol. 54, pp. 3873–3883, Oct 2006.

[4] K. Forsythe, D. Bliss, and G. Fawcett, "Multiple-input multiple-output (MIMO) radar: Performance issues," in *Proc. 38th Asilomar Conf. Signals, Systems and Computers*, Pacific Groove, CA, Nov. 2004, pp. 310–315.

[5] C. Y. Chen and P. P. Vaidyanathan, "MIMO radar spacetime adaptive processing using prolate spheroidal wave functions," *IEEE Trans. Signal Process.*, vol. 56, pp. 623–635, Feb 2008.

[6] N. Lehmann, A. Haimovich, R. Blum, and L. Cimini, "High resolution capabilities of MIMO radar," in *Proc. 40th Asilomar Conf. Signals, Systems and Computers*, Pacific Groove, CA, Nov. 2006, pp. 25–30.

[7] N. Lehmann, E. Fishler, A. Haimovich, R. Blum, D. Chizhik, L. Cimini, and R. Valenzuela, "Evaluation of transmit diversity in MIMO-radar direction finding," *IEEE Trans. Signal Process.*, vol. 55, pp. 2215–2225, May 2007.

[8] E. Fishler, A. Haimovich, R. Blum, L. Cimini, D. Chizhik, and R. Valenzuela, "Spatial diversity in radars - models and detection performance," *IEEE Trans. Signal Process.*, vol. 54, no. 3, pp. 823–838, Mar. 2006.

[9] N. Lehmann, A. Haimovich, R. Blum, and L. Cimini, "MIMO-radar application to moving target detection in homogenous clutter," in *Proc. Adaptive Array Processing Workshop (ASAP)*, MIT Lincoln Laboratory, MA, Jul. 2006.

[10] ——, "MIMO radar moving target detection in homogeneous clutter," to be published.

[11] Q. He, R. Blum, H. Godrich, and A. Haimovich, "Cramer-Rao bound for target velocity estimation in MIMO radar with widely separated antennas," *Information Sciences and Systems CISS 2008 42nd Annual Conference*, pp. 123–127, Mar. 2008.

[12] A. Sheikhi and A. Zamani, "Temporal coherent adaptive target detection for multi-input multi-output radars in clutter," *Radar Sonar and Navigation IET*, pp. 86–96, Apr. 2008.

[13] K. Ward, C. Baker, and S. Watts, "Maritime sureveillance radar. I. Radar scattering from the ocean surface," in *IEE Proc. F*, vol. 137, Apr. 1990, pp. 51–62.

[14] F. Gini, A. Farina, and G. Foglia, "Effects of foliage on the formation of K-distributed SAR imagery," *Signal Processing*, vol. 75, pp. 161–171, Jun. 1999.

[15] M. Greco, F. Bordoni, and F. Gini, "X-band sea-clutter nonstationarity: Influence of long waves," *IEEE J. Ocean. Eng.*, vol. 29, no. 2, pp. 269–283, Apr. 2004.

[16] P. Sammartino, C. Baker, and H. Griffiths, "Adaptive MIMO radar system in clutter," *Radar Conference 2007 IEEE*, pp. 276–281, Apr. 2007.

[17] A. Balleri, A. Nehorai, and J. Wang, "Maximum likelihood estimation for compound-gaussian clutter with inverse gamma texture," *Aerospace and Electronic Systems, IEEE Transactions on*, vol. 43, no. 2, pp. 775–779, 2007.

[18] J. Wang, A. Dogandzic, and A. Nehorai, "Maximum likelihood estimation of compound-gaussian clutter and target parameters," *IEEE Trans. Signal Process.*, vol. 54, no. 10, pp. 3884–3898, Oct. 2006.

[19] A. Dogandzic and A. Nehorai, "Generalized multivariate analysis of variance: A unified framework for signal processing in correlated noise," *IEEE Signal Process. Mag.*, vol. 20, pp. 39–54, Sep. 2003.

[20] C. Liu, D. Rubin, and Y. Wu, "Parameter expansion to accelerate EM: The PX-EM algorithm," *Biometrika*, vol. 85, pp. 755–770, Dec. 1998.

[21] S. M. Kay, *Fundamentals of Statistical Signal Processing: Detection Theory*. Upper Saddle River, NJ: Prentice Hall PTR, 1998.

[22] M. Hurtado and A. Nehorai, "Polarimetric detection of targets in heavy inhomogeneous clutter," *IEEE Trans. Signal Process.*, vol. 54, no. 4, pp. 1349–1361, Apr. 2008.

[23] P. Bickel and K. Doksum, *Mathematical Statistics: Basic Ideas and Selected Topics*, 2nd ed. Upper Saddle River, NJ: Prentice Hall, 2000.